High-Frequency Dynamic Nuclear Polarization NMR for Solids: Part 2 - Development and Applications

Michelle Ha and Vladimir K. Michaelis*

Department of Chemistry, University of Alberta, Edmonton, Alberta, Canada T6G 2G2

*Correspondence: vladimir.michaelis@ualberta.ca

Abstract

High-frequency dynamic nuclear polarization nuclear magnetic resonance (DNP NMR) spectroscopy is having a major impact on the far-reaching abilities of solid-state NMR. This high-sensitivity technique made possible by transferring high polarization from an unpaired electron source to an NMR-active nucleus is rewriting the capabilities of NMR spectroscopy within the chemical sciences. In Part I, we briefly introduced some of the instrumentation, hardware and essentials to apply DNP NMR in solids. Below, we highlight some of the advances in DNP method development, as well as the major breakthroughs within the NMR community made possible by DNP NMR.

Introduction

Solid-state nuclear magnetic resonance (NMR) spectroscopy has been a key analytical technique used in the characterization of atomic- and molecular-level structure in solids for many scientific disciplines. Improving the sensitivity of NMR has been a focus of many since the inception of NMR spectroscopy due to the many limitations of challenging NMR nuclei and chemical problems. In the past decade high-frequency DNP NMR spectroscopy has been evolving rapidly, providing new findings and opening a pathway for once unattainable results.

Although high-frequency DNP NMR spectroscopy is a relatively new subset of solid-state NMR spectroscopy, the concept of transferring the large Boltzmann polarization of unpaired electrons to nearby nuclei was initially proposed by Albert Overhauser in 1953.[1] A few months later, Thomas Carver and Charles Slichter reported experimental evidence *via* ^{7}Li NMR for what is now known and widely used as the Overhauser Effect (OE).[2, 3] These early experiments laid the foundation for the exciting work in DNP for years to come. As the field began to emerge a series of seminal studies and reports appeared throughout the late 1950's to 1980's. These include

discoveries of the solid effect (SE),[4-6] cross effect (CE)[7-11] and thermal mixing (TM).[12] Understanding the various mechanisms aided in directing novel approaches to introduce a high-polarization state in a variety of challenging chemical systems. Unfortunately, a limitation in technology in these early years such as limited field strengths (< 1 T) and the lack of high-frequency microwave sources constrained the true ground-breaking potential of DNP.[13] In the 1980's Robert Wind, Jacob Schaefer, Costantino Yannoni and others began applying DNP to high-resolution magic-angle spinning (MAS) NMR of solids, with the focus on using either the OE or SE since the microwave field strengths were limited (*e.g.,* 60 MHz for ^{1}H and 40 GHz for e^{-}).[12, 14-16] A turning point occurred in the early 1990's when Robert Griffin and co-workers (Francis Bitter Magnet Laboratory, MIT) partnered with Richard Temkin (Plasma Science and Fusion Center, MIT) to initiate the development of high-frequency DNP NMR in efforts to study health-related chemical problems in biomolecular solids. The first 211 MHz / 140 GHz DNP NMR spectrometer was assembled, combining a 5 T superconducting magnet with a robust DNP NMR cryogenic probe, and a continuous-wave high-power 140 GHz gyrotron, all barely emerging technologies at the time.[17, 18] These early studies of high-frequency DNP NMR stimulated the NMR community, resulting in further instrumentation[19-24] and application successes. By 2010, the first commercial DNP NMR system from Bruker Biospin Inc. became available, thereby providing world-wide access to this technology.[25]

As an extension to Part I, this article will introduce an overview of DNP NMR applications within the areas of small molecules, biomolecular solids, materials science and method developments in high-frequency DNP NMR spectroscopy in the last decade. Finally, although this article and Part 1 are by no means exhaustive, the topics provided herein are meant to provide the reader with interest in DNP NMR some direction in identifying varying research themes, breakthroughs and guidance of the available literature.[12, 26-36] As DNP NMR is a

technique that involves transfer of electron polarization to NMR nuclei, we first discuss direct vs. indirect DNP and approaches to measure an enhancements (ε).

Direct and Indirect DNP and the Measurement of ε

A DNP NMR experiment can be done either directly or indirectly using any conventional NMR experiment. In simple terms the only difference between a high-frequency DNP NMR experiment and an NMR experiment is the use of microwaves to enable the transfer of electron polarization (from unpaired electrons) to some NMR-active nucleus. As mentioned in Part 1, direct polarization transfer involves the transfer of electron polarization to the desired NMR active nuclei X (*e.g.*, X= ^{13}C, ^{27}Al, ^{29}Si, ^{17}O, ^{2}H, *etc*.), followed by observation (*i.e.,* e^- to X, then detecting X). Indirect transfer entails the electron polarization being transferred to an intermediate nucleus (typically ^{1}H), followed by a nucleus-nucleus polarization step such as cross-polarization (*i.e.,* e^- to ^{1}H then to X followed by detecting X).

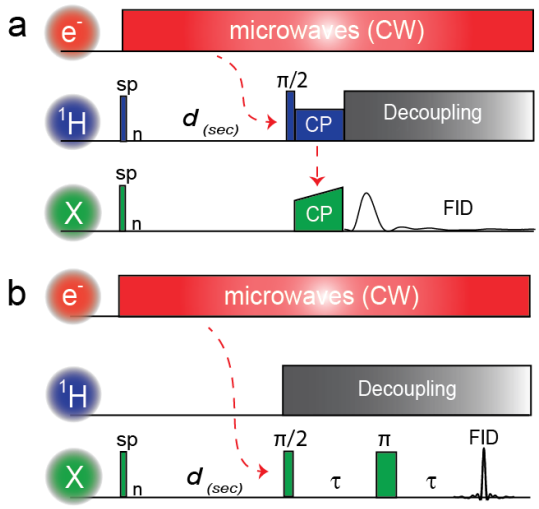

Figure 1: Common DNP NMR pulse programs involving indirect (a) and direct (b) DNP polarization transfer. Continuous microwaves bombarded the sample during the DNP experiment. Upon the e^- - n^0 polarization transfer during a polarization build-up time T_B the high polarization of the NMR-active nuclei can then be read-out performing routine NMR experiments such as cross-polarization (a, indirect) or a Hahn-echo (b, direct) with or without high-power decoupling (e.g., ^{1}H).

Examples of direct and indirect DNP NMR experiments are shown in Figure 1. When microwaves are on, this is a DNP NMR experiment (sometimes denoted as MWon, μwon or DNP), when the microwaves are off, this is a standard NMR experiment (sometimes denoted as MW_{off}, μw_{off} or non-DNP). The DNP enhancement factor, ε (or sometimes ε_{DNP}) can be measured by comparing the signal-to-noise ratio for an NMR spectrum acquired with and without microwaves under identical experimental conditions, as shown in equation 3:

$$\varepsilon = (I_{mwon} / I_{mwoff}) \qquad (3)$$

where I_{mwon} and I_{mwoff} denote the peak intensity with the microwaves on and off, respectively. Occasionally publications attempt to correct for the effect from temperature (*i.e.,* the gain in Boltzmann polarization as the sample is cooled to cryogenic temperatures), using the symbol, ε^t as DNP experiments are typically performed below 120 K, whereas most NMR experiments are performed between 250 and 300 K.

$$\varepsilon^t = (I_{mwon} / I_{mwoff}) \cdot (T_{NMR} / T_{DNP}) \quad (4)$$

Reporting ε (eqn 3), the on/off value is the simplest approach in assessing the enhancement value. However over the last few years, various groups have suggested new approaches for a more accurate description of the enhancement (*vide infra*); two of these are discussed below.

Corzilius *et al*. studied a series of polarizing agents under non-spinning and MAS DNP NMR conditions to assess the effect of the radicals and the DNP NMR process on the overall sensitivity.[37] They propose using the overall sensitivity enhancement, E, which represents the practical sensitivity gain one observes when comparing a DNP experiment with an NMR experiment performed at the same temperature but without a radical.

$$E = \varepsilon \cdot (I/I^o) \cdot (\sqrt{T_1^o}/T_B) \quad (5)$$

Where I and I^o are the off-signal (no microwaves) amplitudes of the sample with and without radical, respectively and, T_B and T_1^o are the spin-lattice relaxation times at the same temperature of the sample with and without radical, respectively.

Takahashi *et al*. proposed the assessment of the real value in performing a DNP NMR experiment and introduced the absolute sensitivity ratio, ASR. According to the authors, the ASR is experimentally determined by comparing the signal-to-noise ratio per unit of square root of time between a DNP experiment and an NMR experiment at "conventional" conditions (*e.g.,* 298 K, no solvents, no radical, *etc*.).

$$ASR = \varepsilon_{DNP} \cdot \varepsilon_T \cdot \eta_{T1} \cdot \chi_{bleach} \cdot \chi_{LW} \cdot \chi_{weight} \cdot \chi_{seq} \cdot \chi_{ex} \quad (6)$$

where ε_T is the gain due to performing the measurement at a low temperature, η_{T1} takes into account the different repetition times, χ_{bleach} is the factor accounting for signal bleaching, χ_{LW} is the ratio of the linewidths, χ_{weight} is the ratio of the effective sample weights, χ_{seq} is the ratio of the

effective magnetization after decays during the experiment and χ_{ex} is the factor accounting for additional effects.[38]

Evaluation of DNP NMR and its effectiveness has been at the root of countless discussions within the NMR community. The approaches presented above are by no means the only ones available as other groups have also weighed in using alternative approaches.[37-42]

Applications of High-Frequency DNP NMR

i. Method Development

Although the concept of DNP and the integration of DNP into high-field NMR is not new, there is still much development needed in the field. Four areas of high-frequency DNP development are discussed below including sedimented-solute DNP (SedDNP), solvent-free DNP, DNP enhancements via transition metal solids and fast MAS DNP.

Sedimented-solute nuclear magnetic resonance (SedNMR) spectroscopy is a method which utilizes the sedimented states of molecules post-ultracentrifugation to examine its structural characteristics which otherwise would not be detectable via solution or MAS NMR.[43] SedDNP is a combination of the SedNMR method and DNP techniques to further enhance signal intensity, as well as to provide an alternative tool for investigating frozen sediment states. In 2013, Ravera *et al.* studied the homo-24-mer ApoF via SedDNP at 5 T and at temperatures below 90 K.[44] In the absence of a typical glass-forming agent, such as glycerol, signal enhancements of $\varepsilon \sim 42 / 22$ (^{1}H, indirect / ^{13}C, direct) were observed from the frozen ApoF sediment. While this experiment demonstrated significant signal enhancements for studying samples via SedDNP, the sedimented proteins exhibited glass-like behaviour which suggests the potential of performing biomolecular DNP experiments in the absence of glass-forming agents.

As discussed in Part I, DNP samples are typically prepared with a glass-forming agent, to protect the sample from the cryogenic temperatures needed in a DNP experiment. However, the formation of the glass prevents the study of some solid-state structures. In a 2013 study by Ong *et al*., amorphous and crystalline *ortho*-terphenyl (OTP), a well-studied organic glass-forming solid, were prepared in the absence of a solvent and subsequently examined via DNP NMR at 5 T.[45] DNP enhancements of $\varepsilon \sim 58$ and $\varepsilon \sim 36$ for amorphous and crystalline samples respectively, were measured for 95% deuterated OTP studied via $^{13}C[^{1}H]$ CP DNP MAS NMR (indirect), as well as via direct ^{13}C polarization studies demonstrating enhancements of $\varepsilon \sim 67$ for the amorphous state and $\varepsilon \sim 50$ for the crystalline state.

Thankamony *et al.* investigated mesoporous silica functionalized with TEMPO via solvent-free DNP and obtained an enhancement of $\varepsilon \sim 3$ via direct ^{29}Si polarization.[46] Although the reported DNP enhancements are quite small for ^{29}Si, the polarization buildups were fast which suggests a significant advantage for DNP experiments performed below 100 K since the sensitivity factors will increase for solids that suffer from long spin-lattice relation times.

While current DNP experiments utilize organic radicals as the polarizing agent, paramagnetic metal ions could potentially be used as a source of polarization as well. This is advantageous for metalloproteins containing paramagnetic metals since they contain an intrinsic source of polarization resulting in additional DNP enhancements. Corzilius *et al.* were interested in DNP enhancements with high-spin transition-metal ions such as Gd^{3+} and Mn^{2+} via the solid effect.[47] When compared to a sample containing a well-established trityl radical, the EPR line widths for the transition metal-ion polarizing agent were narrow and the DNP enhancements were comparable. This demonstrates the possibility of using transition-metal compounds as polarizing agents for DNP experiments via the SE. Furthermore, paramagnetic metals have been successfully applied as polarizing agents by substituting a diamagnetic Co with a Cr

paramagnetic metal centre into an inorganic coordination complex[48] and using a Mn-containing linker within nucleic acids.[49]

While solid-state NMR spectroscopy performed under magic-angle spinning (MAS) is not a new technique, the use of fast MAS (> 20 kHz) in conjunction with DNP-enhanced solid-state NMR is developing rapidly. Currently, the majority of high-field DNP experiments are performed using 3.2 or 4 mm rotors. Although the use of these sizes allows for larger sample volumes, this caps the maximum MAS frequency to ~15 kHz at cryogenic temperatures as dry nitrogen gas becomes denser as it approaches its liquefaction temperature (77 K). *Chaudhari et al.* were interested in the effect of fast MAS (up to 40 kHz) on DNP enhancements.[50] Using a prototype 1.3 mm DNP probe, signal enhancement factors of 56 – 66 were observed over a spinning frequency range of 10 – 40 kHz in bulk solutions of glycine or proline. Additionally, an enhancement of $\varepsilon = 80$ was obtained for a 1.3 mm sapphire rotor at 20 kHz MAS compared to an enhancement of $\varepsilon = 30$ obtained for a 3.2 mm sapphire rotor at 10 kHz MAS (an increase by about a factor 2). Although, overall sensitivity is lost due to the smaller fill-volume of the rotor (*i.e.,* 30 uL (3.2 mm) vs. 2.5 uL (1.3 mm) fill volumes), microwave distribution and penetration depth is improved within smaller samples, leading to a larger enhancement value. Similar effects were reported in 2006 when switching between a 2.5 and 4 mm rotor within the TOTAPOL study by Song et al.[51]

ii. Biomolecular Solids

Solid-state NMR is a powerful structural elucidation tool for biomolecular solids ranging from small peptides and proteins to complex membrane proteins and disordered amyloid fibrils. The atomic-level structural insight afforded by the ability to avoid surfactants and/or high-quality crystals often essential in liquid NMR or diffraction studies, respectively, further enhances its

attraction. Unfortunately the limitation in NMR sensitivity inhibits its full potential. With the advent of higher-field spectrometers and the necessity of multidimensional data for structural elucidation, it is only natural to apply DNP to these chemical systems. As such, a wealth of structural studies has been reported using high-frequency DNP NMR including membrane proteins, microcrystalline systems, amyloid fibrils, enzymes, *etc*.[26-28, 31] The ability to cool a sample and perform DNP NMR offers immense gains in sensitivity allowing one to probe various structural features not possible using conventional methods. One advantage of cooling is that it minimizes dynamics present within a protein enabling the determination of more structural information. At the same time this causes increased spectral crowding, complicated further by some distribution in the dynamic portions of the protein.[52]

In 2014 Fricke *et al.* studied T3SS bacterial needles at 14 T to illustrate the gain in sensitivity, $\varepsilon = 23$ ($^{13}C[^{1}H]$, indirect) (corresponding to a reduction in time by a factor of ~ 500) while maintaining resolution with a full width at half height of ~ 1 ppm.[53] They were able to perform backbone assignments of the protein using common N-C, NCACX and NCOCX-based 2D and 3D experiments. The complex 3D experiments of these highly dilute samples were performed in less than three days and allowed the assignment of many individual peaks leading to nearly 50% of the backbone assignment.

Bayro *et al.* undertook a series of experiments whereby the interstrand architecture could be elucidated in amyloid fibrils, demonstrating this on PI3-SH3.[54] Here they utilized a technique to create a mixed sample whereby monomers were synthesized using either ^{15}N or ^{13}C residues. This approach was initially demonstrated by Debelouchina *et al.* in a two-week experiment in 2010, studying the B2M protein whereby they acquired long-mixing ZF-TEDOR NMR spectra.[55] Using a 400 MHz / 263 GHz DNP NMR instrument the same technique was applied yielding intermolecular contacts in just over a day (Figure 2). Furthermore, with the reduced dynamics

and the gains from DNP NMR, 52 intermolecular cross-peaks were assigned, more than twice as many as was established at 750 MHz (23 contacts were obtained) on the same protein, in 1/10th the time.

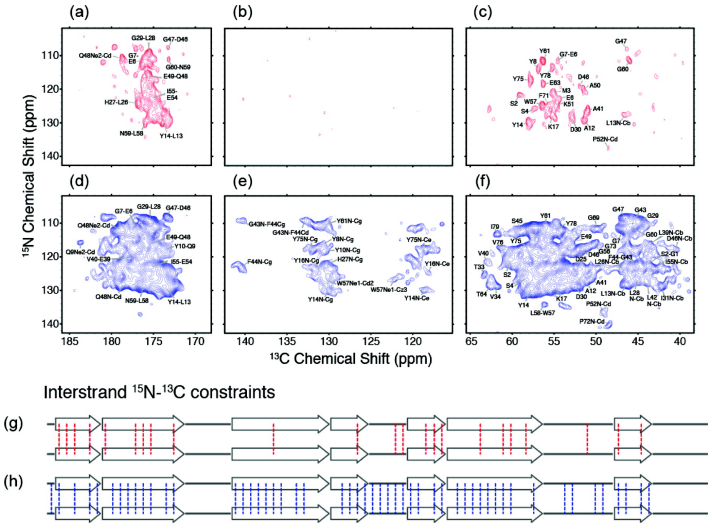

Figure 2: Two-dimensional ^{13}C-^{15}N ZF-TEDOR MAS NMR (red, 16 day acquisition at 750 MHz) and DNP-enhanced (blue, 32 hrs acquisition at 400 MHz, indirect, ^{13}C[^{1}H]) correlation spectra illustrating interstrand contacts within a mixed (^{13}C-only / ^{15}N-only labelled) PI3-SH3 amyloid fibrils sample, by Bayro et al.[54] Reproduced from Bayro, M.J., Debelouchina, G.T., Eddy, M.T., Birkett, N.R., MacPhee, C.E., Rosay, M., Mass, W.E., Dobson, C.M. and Griffin, R.G. Journal of the American Chemical Society 2011, 133(35), 13967-13974. Copyright 2011 American Chemical Society.

In 2013, Gelis *et al.* demonstrated the advantages of combining DNP and MAS NMR for studying ribosomal structural biology.[56] While liquids NMR spectroscopy has been able to provide detailed primary, secondary, tertiary and even quaternary protein information, the sensitivity of ribosomal studies is limited due to the low ribosome concentrations needed to avoid protein aggregation. Additionally, the degradation of such samples after ~24 hours at 25 ^{o}C limits the use of extensive time averaging, typically needed for routine MAS NMR experiments. By altering the sample preparation techniques, such as increasing the concentration of material via direct pelleting of the ribosome subunits into the NMR rotor, DNP enhancement of ^{13}C signals improves (^{1}H, ε~25) such that it becomes feasible to acquire high-quality 2D correlation spectra of ribosome complexes within a practical experimental timeframe. Furthermore, the cryogenic

232 temperature (~ 100 K) utilized in DNP experiments greatly extends the lifetime of the easily
233 degradable samples allowing effective signal averaging.

234 In a 2011 study by Linden *et al.*, the effects of TOTAPOL radical concentration and
235 proximity to nicotinic acetylcholine receptors bound to neurotoxin II were examined.[57] As the
236 concentration of TOTAPOL varied in addition to the proximity to the receptors, the resulting
237 spectra provided higher resolution and signal enhancement overall in comparison to the non DNP
238 spectrum. Lastly, while the conventional 2D ^{13}C-^{13}C correlation spectrum was recorded in nine
239 days, some peaks in the DNP spectrum were better resolved in ~14 hours (~6% of the initial
240 time).

241 DNP NMR has also transitioned to studies of small crystalline molecules, such as those of
242 interest within the pharmaceutical industry, where tracking low-concentration active
243 pharmaceutical ingredients is a challenge. Rossini et al., in 2014 utilized the DNP NMR
244 enhancements to study a series of commercial pharmaceutical formulations of a popular
245 antihistamine, cetirizine dihydrochloride.[58] With the gains provided by DNP they were able to
246 expand beyond ^{13}C NMR, and probe natural abundance ^{15}N using DNP-enhanced $^{15}N[^{1}H]$
247 HETCOR spectra (Figure 3). As the chemical shift range of ^{15}N is larger than that for ^{13}C and
248 often has far fewer correlations, they stated these data lead to clearer structural contacts, offering
249 a new probe nucleus within the field. The DNP NMR technique within pharmaceutical
250 formulations has also recently been extended to ^{35}Cl.[59]

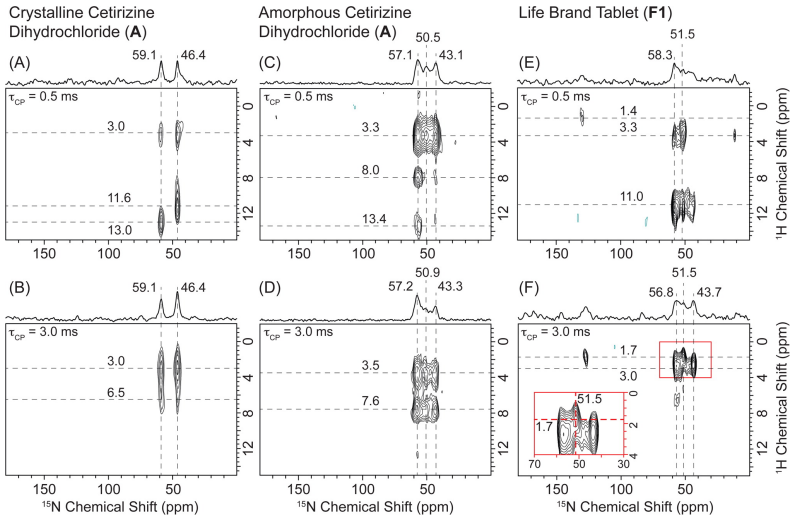

Figure 3: ^{1}H-^{15}N HETCOR DNP-enhanced MAS NMR spectra (indirect, ^{15}N[^{1}H]) of crystalline (A, B, ~0.5 hrs) and amorphous (C, D, ~5 hrs) pure cetirizine dihydrochloride and in formulation (E, F, ~5 hrs), by Rossini et al. at natural abundance (^{15}N).[58] Reproduced from Rossini, A.J., Widdifield, C.M., Zagdoun, A., Lelli, M., Schwarzwälder, M., Copéret, C., Lesage, A. and Emsley, L., Journal of the American Chemical Society 2014, 136(6), 2324-2324. Copyright 2014 American Chemical Society.

iii. Materials Science

As the development of biomolecular DNP NMR progressed and the commercialization of DNP NMR instrumentation enabled the technique to be more readily applied, the materials community quickly adapted the technique for the study of inorganic chemical systems. In particular, the large surface areas and often low concentrations of active sites restricts our understanding of the short- and medium-range structural architecture of materials which exhibit absorption, catalytic, or gas storage functions. The advances provided by DNP are rapidly changing the once common notion of *impossible* to *readily achievable*.

In 2011, Lelli *et al.,* demonstrated the ability to characterize various bonding modes in surface functionalized organic-silica materials using fast 1D and 2D DNP NMR experiments for two different synthetic approaches: (a), attaching phenol moieties directly (sol-gel technique) and (b), indirectly (post-grafting) to the silica surface.[60] Using the sensitivity gains offered by DNP NMR (^{1}H, $\varepsilon \sim 20$), they were able to confirm that the sol-gel process favours phenol-group

incorporation through T^3 sites (Phenol-Si-$(OSi)_3$) while post-grafting leads to a more disordered surface.

Understanding the atomic-level structure of surfaces is difficult, thus creating challenges within the materials science in how to synthetically adjust reaction conditions to promote desired properties. Using both dipolar (through space) and *J*-based (through bond) 2D ^{29}Si-^{29}Si correlation DNP NMR spectroscopy, Lee *et al.*, were able to characterize functionalized Si nanoparticles and their interconnectivities (Figure 4).[61] They showed that clusters of surface silanols as well as T^3-Q^3 units (connected by a bridging oxygen) are present on the surface of these functionalized nanoparticles. This approach is impossible using conventional NMR methods as the transfer efficiencies (< 3%), surface coverage and low natural abundance of ^{29}Si (4.7%) would not provide the needed sensitivity. The gain from DNP therefore offered the ability to apply this technique, gaining extensive understanding of the surface coverage / speciation (*i.e.,* Q^4, Q^3, T^3, *etc*.) providing the needed information for further discovery.

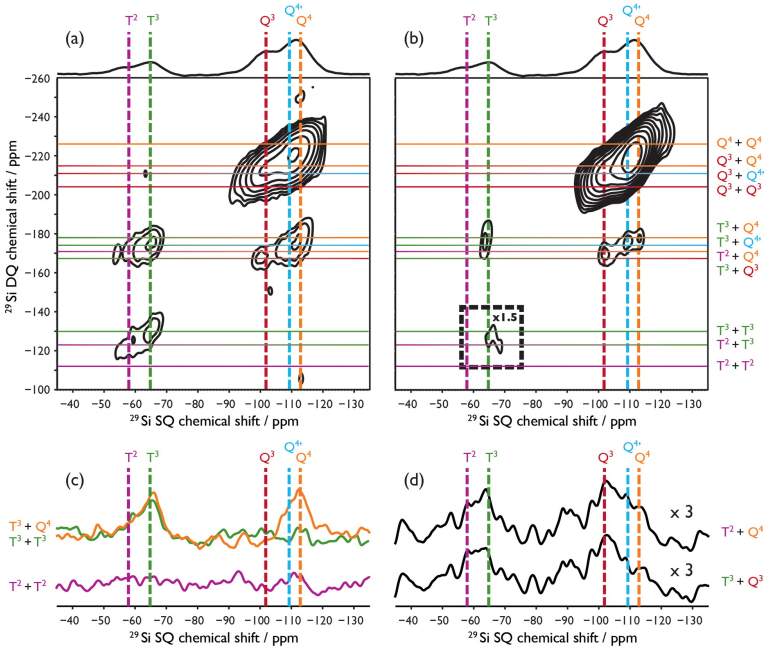

Figure 4: Two-dimensional ^{29}Si-^{29}Si DNP-enhanced MAS NMR (~6 hrs) correlation spectra (indirect, ^{29}Si[^{1}H]) of PES-functionalized silica NPs, by Lee et al. at natural abundance (^{29}Si).[61] Reproduced from Lee, D., Monin, G., Duong, N.T., Lopez, I.Z., Bardet, M., Mareau, V., Gonon, L. and De Paëpe, G. Journal of the American Chemical Society 2014, 136(39), 13781-13788.[61] Copyright 2014 American Chemical Society.

In 2015, Piveteau *et al*. studied the chemistry of colloidal semiconductor nanocrystals, more commonly referred to as quantum dots (QDs), via DNP NMR.[62] Due to the low concentrations of surface sites and the poor sensitivity of NMR spectroscopy, there have been challenges in regards to probing the QD core, QD surface, and capping ligands. For CdSe QDs, distinct signals at −20 and −317 ppm were observed within 32 scans (~ 5 mins) from the QD core and Cd surface species respectively, via DNP NMR. With the ability to clearly resolve all C atom signals within a reasonable timeframe, Piveteau *et al.* were able to acquire DNP enhanced ^{13}C-^{111}Cd 2D correlation spectra overnight, in comparison to an experimental time of > 1000 days for non-DNP-enhanced 2D experiments.

Gunther *et al.* have demonstrated the ability to study low-concentration Sn-active sites within Sn-Beta zeolites, thus obtaining ^{119}Sn[^{1}H] DNP MAS NMR spectra of samples at natural

abundance within hours.[63] Their approach allowed the verification of Sn framework incorporation in various coordination environments (dehydrated and hydrated), and a reliable method in characterizing these catalytic porous materials (Figure 5). In the same year, Emsley and co-workers also utilized the DNP technique to explore active sites within Sn-Beta zeolites[64] and to unravel the structure of ligand-capped Sn-based nanoparticles.[65] Previous to this, nearly all studies on these sorts of materials required expensive ^{119}Sn isotopic enrichment.

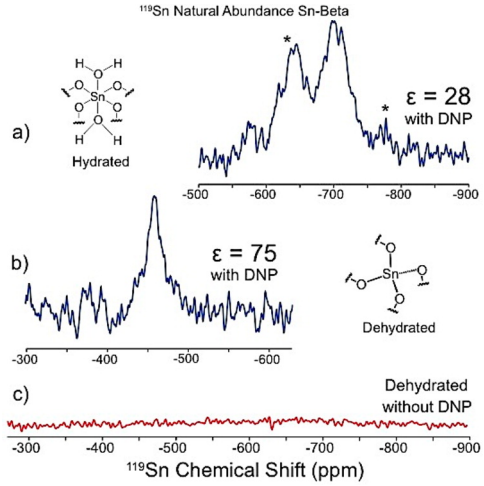

Figure 5: ^{119}Sn DNP-enhanced MAS NMR spectra (indirect, ^{119}Sn[^{1}H]) of hydrated (a, ~18 hrs), dehydrated (b, ~21 hrs) and non-DNP enhanced dehydrated (c, ~250 hrs) Sn-Beta zeolite at natural abundance (^{119}Sn), by Gunther et al. Reproduced from Gunther, W.R., Michaelis, V.K., Caporini, M.A., Griffin, R.G. and Roman-Leshkov, Y., Journal of the American Chemical Society 2014, 136(17), 6219-6222.[63] Copyright 2014 American Chemical Society.

While combining DNP with techniques such as CP and MAS are quite common, other pulse programs are beginning to emerge coupling their capabilities with DNP NMR sensitivity to expand our knowledge of quadrupolar nuclei. For example, oxygen-17 is an extremely rich NMR nucleus within the biological and materials science areas, but is frequently avoided due to its insensitive nature, being quadrupolar and low natural abundance (< 0.04 %). High-frequency DNP NMR has been shown to be effective in polarizing (direct and indirect) oxygen-17 in a range of chemical environments implementing various approaches including CP, CPMG, 2D correlation spectroscopy such as ^{17}O-^{1}H HETCOR and providing distance information using

SEDOR to measure the ^{1}H-^{17}O distances.[31, 66-68] Recently Perras *et al.* obtained signal enhancements between 2 and 11 by using the PRESTO polarization-transfer technique (^{17}O[^{1}H] PRESTO-QCPMG) compared to the familiar CP technique (^{17}O[^{1}H] CP-QCPMG).[69] Additionally, an overall sensitivity enhancement of 5 for natural abundance ^{17}O NMR spectra of $Mg(OH)_2$ and $Ca(OH)_2$ were obtained leading to a decrease in experimental time (from ~1 day for CP-QCPMG to a few hours for PRESTO-QCPMG), enabling 2D acquisition methods such as HETCOR (Figure 6). In a follow-up study, Perras *et al.* probed the interactions between the surface of the silica gel and other molecules, and characterized H-bonded and lone ^{17}O sites on the silica gel surface by examining ^{1}H-^{17}O dipolar oscillations and ^{1}H-^{17}O internuclear distances, respectively.[70]

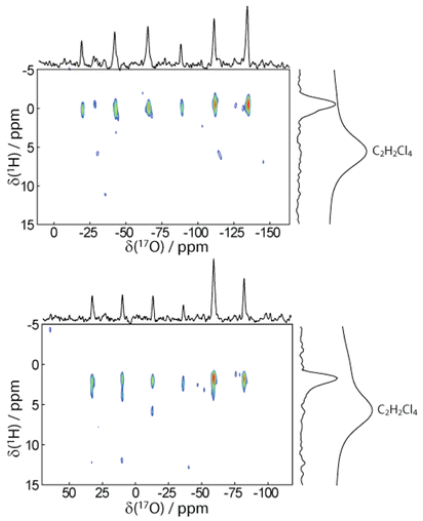

Figure 6: ^{1}H-^{17}O PRESTO-CPMG-HETCOR DNP-enhanced MAS NMR spectra (indirect, ^{17}O[^{1}H]) of $Mg(OH)_2$ (top, ~5 hrs) and $Ca(OH)_2$ (bottom, ~5 hrs) by Perras et al. at natural abundance (^{17}O).[69] Reproduced from Perras, F.A., Kobayashi, T. and Pruski, M., Journal of the American Chemical Society 2015, 137(26), 8336-8339. Copyright 2015 American Chemical Society.

In 2017, Brownbill *et al.* were interested in comparing CE and OE DNP mechanisms on natural abundance ^{17}O $Mg(OH)_2$ at 18.8 T via the CP and PRESTO techniques (^{17}O[^{1}H] indirect polarization) in an ortho-terphenyl glassing agent.[71] Using CE DNP via an indirect polarization transfer, enhancement factors of up to $\varepsilon = 14$ were obtained, whereas enhancements of $\varepsilon = 17$

were obtained via OE DNP. Although CE DNP resulted in lower ε values, the use of a biradical TEKPol yielded a more time efficient data acquisition period when compared to the monoradical BDPA due to a reduction in the build-up time (11 s vs. 31 s). Without the extensive DNP development driving the gains in sensitivity and subsequent decrease in experimental times, these types of experiments would simply not be possible.

Another example demonstrating the gains in NMR sensitivity is the study of natural abundance ^{43}Ca of carbonated hydroxyapatite (C-HAp), an organic-mineral interface in bone tissues.[72] With a natural abundance of 0.14%, a frequency ratio ($\gamma_{Ca\text{-}43}/\ \gamma_{H\text{-}1}$) of ~6.7% and quadrupolar nuclear spin, I=7/2, ^{43}Ca studies have proven difficult without large sample volumes and selective ^{43}Ca-labelling. In 2017, Lee *et al.* studied the differentiation of surface and core species of natural abundance hydroxyapatite nanoparticles using a combination of MAS NMR and DNP NMR spectroscopy. Using DNP-enhanced CPMAS NMR (indirect, ^{43}Ca[^{1}H]), a reduction in experimental time (< 1 hour for DNP-enhanced CPMAS vs. > 5.5 hours for double-frequency sweep NMR) and an enhancement factor of 15 was obtained for a 1D ^{43}Ca MAS NMR experiment. With the ability to acquire promising 1D DNP-enhanced spectra within a reasonable timeframe, more complex experiments (such as 2D HETCOR) were feasible. Using a limited amount ~~mass~~ of natural abundance sample (~30 mg), Lee *et al.* obtained DNP enhanced HETCOR spectra of C-Hap within 15 hours (in comparison to ~150 days acquisition using conventional NMR). This allowed for differentiation between surface and core Ca^{2+} species and thus expanded the avenues for detailed studies of Ca^{2+} interfaces in bone tissues.

^{17}O and ^{43}Ca are not the only quadrupolar nuclei to be impacted by DNP as a host of others have benefitted from the boost in sensitivity including ^{27}Al, ^{51}V, ^{35}Cl, ^{59}Co, ^{14}N, ^{2}H among others.[31, 48, 59, 66-69, 73-78]

DNP studies showing sensitivity enhancements of 1-2 orders of magnitude have been readily achieved for mesoporous materials without surfactants. However, Lafon *et al.* were interested in mesoporous silica nanoparticles loaded with surfactants since such particles can be tailored toward a wide variety of applications (i.e. drug delivery, sensors, and catalysis).[79] Since the TOTAPOL radical is unable to penetrate into the surfactant-filled mesopores, relatively low enhancements of ~8.2 and ~7.5 for ^{13}C and ^{29}Si signals respectively, were obtained. Although the mesoporous silica nanoparticle produce enhancements that are much smaller than the DNP enhancements shown previously for dry mesoporous silica (ε ~30 ($^{13}C[^{1}H]$) and ε ~32, ($^{29}Si[^{1}H]$), indirect), Lafon *et al.* were able to produce consistent results in comparison to predictions based on one-dimensional ^{1}H spin diffusion modeling and thus illustrated the potential for the study of organic-inorganic hybrid materials using DNP.

Summary and Future Outlook

The far-reaching abilities of DNP NMR appear to be vast and will undoubtedly continue in the coming years. In 2010, Griffin and Prisner[13] stated that DNP NMR is undergoing a renaissance, transitioning from low to high fields and frequencies. Less than a decade after that special DNP NMR issue,[13] high-frequency DNP NMR spectroscopy has entered a stage analogous to that experienced during the *Industrial Revolution*. This will evidently expand as available technology will continue to advance in magnetic field strength (high to ultrahigh magnetic fields moving toward 1.1 to 1.3 GHz), the ability of MAS technology (fast to ultrafast moving beyond 100 kHz), electronics (hardware that is low noise, has a smaller footprint and faster responses), newer experimental approaches (pulse sequences and multidimensional, non-uniform sampling) and the availability of commercially available DNP infrastructure (400, 600 and 800 MHz currently on the market). This article has only captured a few advances in

application and development over the past few years. As the technique continues to develop, solid-state NMR experiments once considered impossible will become routine, offering exciting opportunities for advances in many research fields.

Acknowledgements

VKM acknowledges the Natural Sciences and Engineering Research Council of Canada (NSERC) Discovery Grants program and the University of Alberta for funding. MH is partially supported by the Government of Alberta Queen Elizabeth II Graduate Scholarship.

References

1. A. W. Overhauser, *Phys Rev*, 1953, **92**, 411-415.
2. T. R. Carver and C. P. Slichter, *Phys Rev*, 1953, **92**, 212-213.
3. T. R. Carver and C. P. Slichter, *Phys Rev*, 1956, **102**, 975-980.
4. A. Abragam and W. G. Proctor, *Cr Hebd Acad Sci*, 1958, **246**, 2253-2256.
5. C. D. Jeffries, *Phys Rev*, 1957, **106**, 164-165.
6. E. Erb, J. L. Motchane and C. R. Ubersfeld, *Acad. Sci.*, 1958, **246**, 2253.
7. A. V. Kessenikh, V. I. Lushchikov, A. A. Manenkov and Y. V. Taran, *Sov Phys-Sol State*, 1963, **5**, 321-329.
8. A. V. Kessenikh, A. A. Manenkov and G. I. Pyatnitskii, *Sov Phys-Sol State*, 1964, **6**, 641-643.
9. C. F. Hwang and D. A. Hill, *Phys Rev Lett*, 1967, **19**, 1011.
10. C. F. Hwang and D. A. Hill, *Phys Rev Lett*, 1967, **18**, 110.
11. D. S. Wollan, *Phys Rev B*, 1976, **13**, 3671-3685.
12. R. A. Wind, M. J. Duijvestijn, C. Vanderlugt, A. Manenschijn and J. Vriend, *Progress in Nuclear Magnetic Resonance Spectroscopy*, 1985, **17**, 33-67.
13. R. G. Griffin and T. F. Prisner, *Physical Chemistry Chemical Physics*, 2010, **12**, 5737-5740.
14. M. Afeworki and J. Schaefer, *Macromolecules*, 1992, **25**, 4092-4096.
15. R. A. Wind, *eMagRes*, 2007.
16. G. G. Maresch, R. D. Kendrick, C. S. Yannoni and M. E. Galvin, *J Magn Reson*, 1989, **82**, 41-50.
17. L. R. Becerra, G. J. Gerfen, B. F. Bellew, J. A. Bryant, D. A. Hall, S. J. Inati, R. T. Weber, S. Un, T. F. Prisner, A. E. Mcdermott, K. W. Fishbein, K. E. Kreischer, R. J. Temkin, D. J. Singel and R. G. Griffin, *J Magn Reson Ser A*, 1995, **117**, 28-40.
18. G. J. Gerfen, L. R. Becerra, D. A. Hall, R. G. Griffin, R. J. Temkin and D. J. Singel, *J Chem Phys*, 1995, **102**, 9494-9497.
19. A. C. Torrezan, S.-T. Han, I. Mastovsky, M. A. Shapiro, J. R. Sirigiri, R. J. Temkin, A. B. Barnes and R. G. Griffin, *IEEE Transactions on Plasma Science*, 2010, **38**, 1150-1159.
20. V. S. Bajaj, M. K. Hornstein, K. E. Kreischer, J. R. Sirigiri, P. P. Woskov, M. L. Mak-Jurkauskas, J. Herzfeld, R. J. Temkin and R. G. Griffin, *J Magn Reson*, 2007, **189**, 251-279.
21. A. B. Barnes, E. Markhasin, E. Daviso, V. K. Michaelis, E. A. Nanni, S. K. Jawla, E. L. Mena, R. DeRocher, A. Thakkar, P. P. Woskov, J. Herzfeld, R. J. Temkin and R. G. Griffin, *J Magn Reson*, 2012, **224**, 1-7.
22. S. Jawla, E. Nanni, M. Shapiro, I. Mastovsky, W. Guss, R. Temkin and R. Griffin, 2011.

23. V. S. Bajaj, C. T. Farrar, M. K. Hornstein, I. Mastovsky, J. Vieregg, J. Bryant, B. Eléna, K. E. Kreischer, R. J. Temkin and R. G. Griffin, *J Magn Reson*, 2003, **160**, 85-90.
24. S. Jawla, M. Reese, C. George, C. Yang, M. Shapiro, R. Griffin and R. Temkin, 2016.
25. M. Rosay, L. Tometich, S. Pawsey, R. Bader, R. Schauwecker, M. Blank, P. M. Borchard, S. R. Cauffman, K. L. Felch, R. T. Weber, R. J. Temkin, R. G. Griffin and W. E. Maas, *Physical Chemistry Chemical Physics*, 2010, **12**, 5850-5860.
26. A. B. Barnes, G. D. Paëpe, P. C. A. v. d. Wel, K.-N. Hu, C.-G. Joo, V. S. Bajaj, M. L. Mak-Jurkauskas, J. R. Sirigiri, J. Herzfeld, R. J. Temkin and R. G. Griffin, *Applied Magnetic Resonance*, 2008, **34**, 237-263.
27. Q. Z. Ni, E. Daviso, T. V. Cana, E. Markhasin, S. K. Jawla, R. J. Temkin, J. Herzfeld and R. G. Griffin, *Accounts of Chemical Research*, 2013, **46**, 1933-1941.
28. T. Maly, G. T. Debelouchina, V. S. Bajaj, K. N. Hu, C. G. Joo, M. L. Mak-Jurkauskas, J. R. Sirigiri, P. C. A. van der Wel, J. Herzfeld, R. J. Temkin and R. G. Griffin, *J Chem Phys*, 2008, **128**, 052211.
29. A. J. Rossini, A. Zagdoun, M. Lelli, A. Lesage, C. Copéret and L. Emsley, *Accounts of Chemical Research*, 2013, **46**, 1942-1951.
30. Y. Su, L. Andreas and R. G. Griffin, *Annual Review of Biochemistry*, 2015, **84**, 465-497.
31. V. K. Michaelis, T.-C. Ong, M. K. Kiesewetter, D. K. Frantz, J. J. Walish, E. Ravera, C. Luchinat, T. M. Swager and R. G. Griffin, *Israel Journal of Chemistry*, 2014, **54**, 207-221.
32. V. A. Atsarkin, *Spv. Phys. Usp.*, 1978, **21**, 725.
33. A. Abragam and M. Goldman, *Nuclear Magnetism: Order and Disorder*, Clarendon Press, Oxford, 1982.
34. M. L. Mak-Jurkauskas and R. G. Griffin, *eMagRes*, 2007.
35. C. D. Jeffries, *Dynamic Nuclear Orientation*, Interscience Publishers, 1963.
36. T. C. Ong, R. Verel and C. Copéret, in *Encyclopedia of Spectroscopy and Spectrometry (Third Edition)*, eds. G. E. Tranter and D. W. Koppenaal, Academic Press, Oxford, 2017, DOI: http://dx.doi.org/10.1016/B978-0-12-409547-2.12130-4, pp. 121-127.
37. B. Corzilius, L. B. Andreas, A. A. Smith, Q. Z. Ni and R. G. Griffin, *J Magn Reson*, 2014, **240**, 113-123.
38. H. Takahashi, D. Lee, L. Dubois, M. Bardet, S. Hediger and G. De Paëpe, *Angewandte Chemie International Edition*, 2012, **51**, 11766-11769.
39. D. Lee, S. Hediger and G. De Paëpe, *Solid State Nuclear Magnetic Resonance*, 2015, **66–67**, 6-20.

40. T. Kobayashi, O. Lafon, A. S. Lilly Thankamony, I. I. Slowing, K. Kandel, D. Carnevale, V. Vitzthum, H. Vezin, J.-P. Amoureux, G. Bodenhausen and M. Pruski, *Physical Chemistry Chemical Physics*, 2013, **15**, 5553-5562.
41. S. Lange, A. H. Linden, Ü. Akbey, W. Trent Franks, N. M. Loening, B.-J. v. Rossum and H. Oschkinat, *J Magn Reson*, 2012, **216**, 209-212.
42. K. R. Thurber and R. Tycko, *The Journal of Chemical Physics*, 2014, **140**, 184201.
43. I. Bertini, C. Luchinat, G. Parigi and E. Ravera, *Accounts of Chemical Research*, 2013, **46**, 2059-2069.
44. E. Ravera, B. Corzilius, V. K. Michaelis, C. Rosa, R. G. Griffin, C. Luchinat and I. Bertini, *J. Am. Chem. Soc.*, 2013, **134**, 1641-1644.
45. T. C. Ong, M. L. Mak-Jurkauskas, J. J. Walish, V. K. Michaelis, B. Corzilius, A. A. Smith, A. M. Clausen, J. C. Cheetham, T. M. Swager and R. G. Griffin, *J Phys Chem B*, 2013, **117**, 3040-3046.
46. A. S. L. Thankamony, O. Lafon, X. Lu, F. Aussenac, M. Rosay, J. Trébosc, H. Vezin and J.-P. Amoureux, *Applied Magnetic Resonance*, 2012, **43**, 237-250.
47. B. Corzilius, A. A. Smith, A. B. Barnes, C. Luchinat, I. Bertini and R. G. Griffin, *J Am Chem Soc*, 2011, **133**, 5648-5651.
48. B. Corzilius, V. K. Michaelis, S. Penzel, E. Ravera, A. A. Smith, C. Luchinat and R. G. Griffin, *J Am Chem Soc*, 2014, **136**, 11716-11727.
49. P. Wenk, M. Kaushik, D. Richter, M. Vogel, B. Suess and B. Corzilius, *Journal of Biomolecular NMR*, 2015, **63**, 97-109.
50. S. R. Chaudhari, P. Berruyer, D. Gajan, C. Reiter, F. Engelke, D. L. Silverio, C. Coperet, M. Lelli, A. Lesage and L. Emsley, *Physical Chemistry Chemical Physics*, 2016, **18**, 10616-10622.
51. C. S. Song, K. N. Hu, C. G. Joo, T. M. Swager and R. G. Griffin, *J Am Chem Soc*, 2006, **128**, 11385-11390.
52. A. B. Siemer, K.-Y. Huang and A. E. McDermott, *PLOS ONE*, 2012, **7**, e47242.
53. P. Fricke, J.-P. Demers, S. Becker and A. Lange, *ChemPhysChem*, 2014, **15**, 57-60.
54. M. J. Bayro, G. T. Debelouchina, M. T. Eddy, N. R. Birkett, C. E. MacPhee, M. Rosay, W. E. Maas, C. M. Dobson and R. G. Griffin, *J. Am. Chem. Soc.*, 2011, **133**, 13967–13974.
55. G. T. Debelouchina, G. W. Platt, M. J. Bayro, S. E. Radford and R. G. Griffin, *J. Am. Chem. Soc.*, 2010, **132**, 17077–17079.
56. I. Gelis, V. Vitzthum, N. Dhimole, M. A. Caporini, A. Schedlbauer, D. Carnevale, S. R. Connell, P. Fucini and G. Bodenhausen, *J Biomol NMR*, 2013, **56**, 85-93.
57. A. H. Linden, S. Lange, W. T. Franks, U. Akbey, E. Specker, B. J. v. Rossum and H. Oschkinat, *J. Amer. Chem. Soc.*, 2011, **133**, 19266–19269.

58. A. J. Rossini, C. M. Widdifield, A. Zagdoun, M. Lelli, M. Schwarzwälder, C. Copéret, A. Lesage and L. Emsley, *J Am Chem Soc*, 2014, **136**, 2324-2334.
59. D. A. Hirsh, A. J. Rossini, L. Emsley and R. W. Schurko, *Physical Chemistry Chemical Physics*, 2016, **18**, 25893-25904.
60. M. Lelli, D. Gajan, A. Lesage, M. A. Caporini, V. Vitzthum, P. Mieville, F. Heroguel, F. Rascon, A. Roussey, C. Thieuleux, M. Boualleg, L. Veyre, G. Bodenhausen, C. Coperet and L. Emsley, *J. Am. Chem. Soc.*, 2011, **133**, 2104-2107.
61. D. Lee, G. Monin, N. T. Duong, I. Z. Lopez, M. Bardet, V. Mareau, L. Gonon and G. De Paëpe, *J Am Chem Soc*, 2014, **136**, 13781-13788.
62. L. Piveteau, T.-C. Ong, A. J. Rossini, L. Emsley, C. Copéret and M. V. Kovalenko, *J Am Chem Soc*, 2015, **137**, 13964-13971.
63. W. R. Gunther, V. K. Michaelis, M. A. Caporini, R. G. Griffin and Y. Román-Leshkov, *J Am Chem Soc*, 2014, **136**, 6219-6222.
64. P. Wolf, M. Valla, A. J. Rossini, A. Comas-Vives, F. Núñez-Zarur, B. Malaman, A. Lesage, L. Emsley, C. Copéret and I. Hermans, *Angewandte Chemie International Edition*, 2014, **53**, 10179-10183.
65. L. Protesescu, A. J. Rossini, D. Kriegner, M. Valla, A. de Kergommeaux, M. Walter, K. V. Kravchyk, M. Nachtegaal, J. Stangl, B. Malaman, P. Reiss, A. Lesage, L. Emsley, C. Copéret and M. V. Kovalenko, *ACS Nano*, 2014, **8**, 2639-2648.
66. V. K. Michaelis, B. Corzilius, A. A. Smith and R. G. Griffin, *J Phys Chem B*, 2013, **117**, 14894-14906.
67. V. K. Michaelis, E. Markhasin, E. Daviso, J. Herzfeld and R. G. Griffin, *The Journal of Physical Chemistry Letters*, 2012, **3**, 2030-2034.
68. F. Blanc, L. Sperrin, D. A. Jefferson, S. Pawsey, M. Rosay and C. P. Grey, *J Am Chem Soc*, 2013, **135**, 2975-2978.
69. F. A. Perras, T. Kobayashi and M. Pruski, *J Am Chem Soc*, 2015, **137**, 8336-8339.
70. F. A. Perras, U. Chaudhary, I. I. Slowing and M. Pruski, *The Journal of Physical Chemistry C*, 2016, **120**, 11535-11544.
71. N. J. Brownbill, D. Gajan, A. Lesage, L. Emsley and F. Blanc, *Chemical Communications*, 2017, **53**, 2563-2566.
72. D. Lee, C. Leroy, C. Crevant, L. Bonhomme-Coury, F. Babonneau, D. Laurencin, C. Bonhomme and G. De Paëpe, *Nature Communications*, 2017, **8**, 14104.
73. T. Maly, L. B. Andreas, A. A. Smith and R. G. Griffin, *Physical Chemistry Chemical Physics*, 2010, **12**, 5872-5878.

74. V. Vitzthum, M. A. Caporini and G. Bodenhausen, *J Magn Reson*, 2010, **205**, 177-179.
75. V. Vitzthum, P. Mieville, D. Carnevale, M. A. Caporini, D. Gajan, C. Coperet, M. Lelli, A. Zagdoun, A. J. Rossini and A. Lesage, *Chemical Communications*, 2012, **48**, 1988-1990.
76. D. Lee, N. T. Duong, O. Lafon and G. De Paëpe, *The Journal of Physical Chemistry C*, 2014, **118**, 25065-25076.
77. D. Lee, H. Takahashi, A. S. L. Thankamony, J.-P. Dacquin, M. Bardet, O. Lafon and G. D. Paëpe, *J Am Chem Soc*, 2012, **134**, 18491-18494.
78. A. J. Perez Linde, D. Carnevale, P. Miéville, A. Sienkiewicz and G. Bodenhausen, *Magnetic Resonance in Chemistry*, 2015, **53**, 88-92.
79. O. Lafon, A. S. L. Thankamony, T. Kobayashi, D. Carnevale, V. Vitzthum, I. I. Slowing, K. Kandel, H. Vezin, J.-P. Amoureux, G. Bodenhausen and M. Pruski, *The Journal of Physical Chemistry C*, 2013, **117**, 1375-1382.